Available online at www.sciencedirect.com
SCIENCE DIRECT
Journal of Molecular Catalysis A: Chemical 244 (2006) 11–19
JOURNAL OF MOLECULAR CATALYSIS A: CHEMICAL
www.elsevier.com/locate/molcata

DFT studies on the location and acid strength of Brönsted acid sites in MCM-22 zeolite

Danhong Zhou [a,b,*], Ying Bao [a], Mingmei Yang [b], Ning He [a], Gang Yang [b]

[a] *Institute of Chemistry for Functionalized Materials, Department of Chemistry, Liaoning Normal University, 850 Huanghe Road, Dalian 116029, China*
[b] *State Key Laboratory of Catalysis, Dalian Institute of Chemical Physics, Chinese Academy of Sciences, 457 Zhongshan Road, Dalian 116023, China*

Received 16 July 2005; received in revised form 22 August 2005; accepted 22 August 2005
Available online 10 October 2005

Abstract

Density functional theory was applied to study the location and the acid strength of Brönsted acid sites in MCM-22 zeolite. The calculations were performed based on cluster model by using of B3LYP hydride functional and 6-31G** basis set. The replacements of Si by Al at eight inequivalent tetrahedral crystallographic sites and the corresponding Si(OH)Al sites were examined by calculating the (Al,H)/Si substitution energy, deprotonation energy, hydroxyl stretching vibtational frequency and the adsorption energy of some basic probe molecules on the acid centers. According to the calculated results it was predicated that the most favorable sites for framework Al substitutions in MCM-22 were T1, T3, and T4 sites and the most preferable Brönsted acid sites were on Al1(O3H)Si4, Al4(O3H)Si1, and Al3(O11H)Si2 bridged groups. The first two acid sites located on the 12-membered ring in the supercages, and the third located in the10-membered ring sinusoidal channels. Evaluating of acid strength by the calculated ammonia adsorption energies revealed that Al1(O3H)Si4 and Al4(O3H)Si1 sites display the similar acidity, and that stronger than Al3(O11H)Si2. The calculated hydroxyl vibrational frequencies of three acid sites were 3628 cm^{-1}, 3618 cm^{-1}, and 3592 cm^{-1}(corrected with scaling factor 0.948), respectively, consistent with the reported FTIR experimental data. It was clarified that the calculations of deprotonation energy and hydroxyl stretching frequency were strongly dependent on the lattice configuration surrounding the Si(OH)Al acid center, therefore, it was obscure using these properties to characterize the acidities from site to site. Nevertheless, adsorption energy of probe molecule on zeolite cluster with adequate size would reflect practically the acid strength corresponding to different zeolite structures.

Keywords: DFT calculations; MCM-22 zeolite; Al substitution; Brönsted acid site; Acidity

1. Introduction

MCM-22 possesses a unique crystal structure containing two independent pore systems [1]. One of the channel systems contains two-dimensional sinusoidal 10-MR (member ring) channels, while the other system consists of large supercages (12-MR) with dimensions 7.1 Å × 7.1 Å × 18.1 Å. The supercages stack one above another through double prismatic six-member rings and are accessed by slightly distorted elliptical 10-MR connecting channels. In general, the synthesized MCM-22 zeolites crystallized as very thin plates with an extremely large external surface area [2,3], on which distributed the 12-MR pockets. The protonic form of MCM-22 is an active catalyst for many reactions requiring acidic sites such as catalytic cracking, olefin isomerization, conversion of paraffins to olefins and aromatics, and alkylation of paraffins with light olefins [4–8]. Indubitably, the acidity (number, location, and strength of the acid sites) plays an important role in the catalysis. Recently, Mo loaded MCM-22 catalyst has been shown to be an excellent catalyst for methane dehydroaromatization with higher benzene selectivity than Mo/HZSM-5 catalyst [9]. Many studies have revealed that MCM-22 behaves like both 10- and 12-MR zeolites [5,8,10–12].

A number of studies have been carried out for locating framework aluminum atoms and the Brönsted acid (B-acid) sites of MCM-22 by using solid-state NMR and FTIR characteristics [13–23]. Upon ^{27}Al MAS NMR experiments, Kennedy et al. [13] had identified three kinds of framework Al atom and Ma et al. [23] found four kinds of framework tetrahedral Al atoms existing in different chemical and crystallographic environments or in different pore systems. The location of protonic acid sites was also discussed from FTIR technologies. Four hydroxyl bands were detected in IR spectrum of pure MCM-22 samples

* Corresponding author. Tel.: +86 411 4216763; fax: +86 411 84258088.
E-mail address: dhzhou@dicp.ac.cn (D. Zhou).

1381-1169/$ – see front matter © 2005 Elsevier B.V. All rights reserved.
doi:10.1016/j.molcata.2005.08.034

and that of low temperature adsorption with weakly basic probe molecules such as CO, NH_3, and pyridine [20,24–25]. The large band centered at 3626 cm^{-1} was resolved into two single components at 3628 cm^{-1} and 3618 cm^{-1} which were assigned to Si(OH)Al groups located in supercages and in sinusoidal channels. The shoulder at 3585 cm^{-1} was attributed to Si(OH)Al groups positioned in a hexagonal prism between two supercages [25]. The fourth component (3670 cm^{-1}) was ascribed to the AlOH groups linked to extraframework Al species.

Theoretical calculations [26–31] are very useful for studying the energetics of substitution of aluminum for silicon at different T sites, and also for the prediction of acid strength, stability, and the possible location of Brönsted acid sites (B-acid) in zeolites. A lot of theoretical calculations have made contributions for sitting framework Al atoms in ZSM-5 zeolite [26,29–34].

A few of theoretical calculation studies were carried out for MCM-22 zeolite. Sastre et al. [35] have performed the theoretical calculations on the substitution energy of aluminum at distinct T sites and the stretching frequency of bridged hydroxyls in MCM-22 by using atomistic simulation techniques. A stronger acidity was predicted for the centers located in supercages. However, the calculated energies of acid centers were only approximate, and the calculations based on quantum chemistry would be needed to obtain more accurate results. Wang et al. [36] have made DFT calculations on the proton hopping inside MCM-22 zeolite. They also studied the acidity on the external surface of MCM-22 zeolite with triphenylphosphine as basic probe using both ^{31}P MAS NMR measurement and MM/QM calculations [37]. Their works have confirmed the existence of protonic acid on the external surface of MCM-22 correlating to T1(O3)T4 B-acid sites.

In this work, density functional theory (DFT) is used to study the framework Al substitutions, the location and the strength of B-acids in MCM-22 zeolite. B3LYP/6-31G** method was used and the calculations were performed on 5T and 8T models. From the calculations it is proposed that the favorite sites for Al substitution are assigned to T1, T3, and T4 sites, whereas the least favorite site is found at T2. The preferred B-acid sites may exist on Al1(O3H)Si4, Al4(O3H)Si1, and Al3(O11H)Si2 bridged groups. The strength of protonic acid is evaluated based on the calculations of proton affinity, atomic charge on proton, hydroxyl stretching vibrational frequency, and the interaction energy with different basic molecules. In addition, the influences of the lattice configuration surrounding the acid center on Brönsted acidity are discussed.

2. Models and methodology

The refined hexagonal *P*6/*mmm* structure of pure silica MCM-22 from Leonowicz et al. [1] was used for calculations. There are eight inequivalent T sites in a unit cell of MCM-22 zeolite, the labeling of which (see Fig. 1) is refined from the *Atlas of Zeolite Framework Types* [38]. Aluminium atom was introduced in each of eight inequivalent T positions, and producing four bridging hydroxyl Si(OH)Al for each Al site. Small cluster model of 5T in $T(OSiH_3)_4$ form was firstly used to do a coarse research. And then 8T cluster model in $(H_3SiO)_3TOT(OSiH_3)_3$ form was used for accurate studies. The models were cut from the crystallographic structure of MCM-22. The dangling Si atoms were terminated by H atoms along the bond direction of next lattice oxygen atoms with a distance of 1.46 Å. Terminating of Si with OH was found not possible because some framework oxygen atoms are shared with two Si atoms. During geometric optimizations the Cartesian positions of terminal silyl groups were held fixed in their crystallographic positions to retain the zeolite structure, while other lattice atoms relaxed. To avoid a distortion of lattice structure, the bridge oxygen atom in TOT angle of 180° in the cluster models was held fixed during the optimizations.

All calculations in this work were carried out with Gaussian 98 program package [39]. We used hydride B3LYP exchange correlation functional for all calculations. It was shown that the hydride DFT methods such as B3LYP give more accurate results for zeolite calculations, especially for the system including hydrogen bonds and weak interactions [40,41]. They have also been shown to predict O–H vibrational frequencies of comparable accuracy to experimental data [42–45]. The basis set used for all elements was 6-31G**.

3. Results and discussion

3.1. Substitution energy of framework Al atom

The structure of MCM-22 showing eight different T sites is shown in Fig. 1. T1 and T4 locate on 12-MR of supercages and

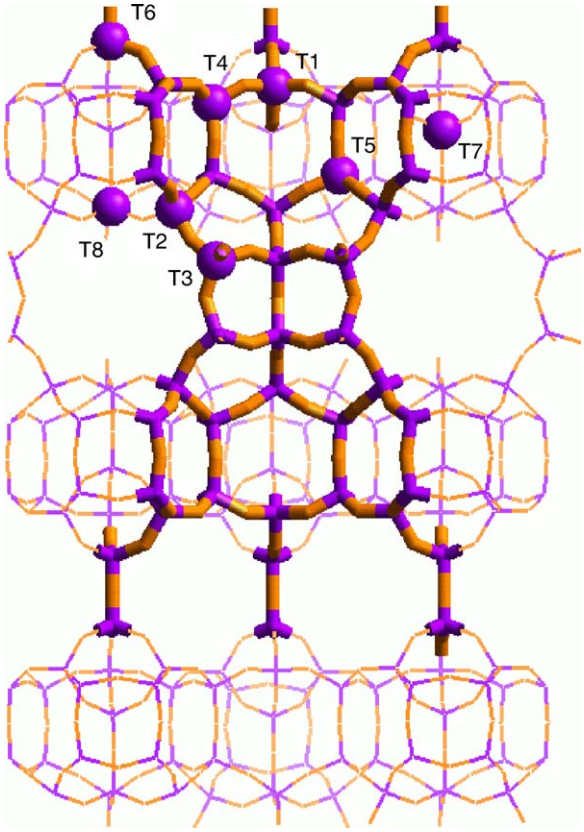

Fig. 1. Structural model of MCM-22 showing the eight different T sites.

T2, T3, and T8 locate in 10-MR sinusoidal systems with T2, T3 connecting to the bottom of supercages. T5 exists on the inner wall of supercages, and T6 locates in the 10-MR connecting channels with a T6–O–T6 angle of 180°. The only one T site embedded inside the framework pocket is attributed to T7, which is inaccessible to the reactant molecules and excluded from our calculations. Substitution of Al(III) to framework Si(IV) results in the changes of lattice geometry and introduce a negative charge. For compensation, the proton can be introduced on one of four oxygen atoms adjacent to Al. In order to avoid the collapse of the zeolite framework, T6 site would not be considered for Al substitution taking into account its TOT angle of 180°. Moreover, some bridged O–H groups are inaccessible by reactants because they locate inside the framework or point to zeolite lattice, and were also excluded from our calculations.

The substitution energy, E_i(Al,H)/Si, was determined by comparing the energy of relaxed Si cluster model with that of

$$E_i(\mathrm{Al,H})/\mathrm{Si} = E[\mathrm{T}_i(\mathrm{Al,H})] - E[(\mathrm{T}_i(\mathrm{Si})]$$

corresponding relaxed (Al,H) cluster model. The lower the E_i(Al,H)/Si, the more stable the B-acid site, and therefore the more favorable for locations of framework Al atoms and Si(OH)Al bridged groups.

Firstly, a rough approach searching the possible B-acid sites was carried out based on 5T model in order to economize the enormous computations. Upon this basis further detailed studies with 8T model were performed. The preliminary results showed that the highest E_i(Al,H)/Si was found on Al5(O8H)Si5. All bridged groups involving Al2 site gave higher E_i(Al,H)/Si, indicating that T2 site is unfavorable for the localization of Al. According to the calculated E_i(Al,H)/Si, we can propose that the preferred location of framework Al atoms are at T1, T3, T4, and T5 sites. The resulted corresponding Si(OH)Al species can be sorted into three groups according to their stabilities. The first group with best stability includes Al1(O3H)Si4, Si1(O3H)Al4, and Si2(O11H)Al3 sites, their relative substitution energies referenced to Al5(O8H)Si5 site, ΔE_i, were −66 kJ/mol, −58 kJ/mol, and −47 kJ/mol, respectively. The second group with middle stability is consisted of Al1(O2H)Si6, Si4(O6H)Al5 and Si2(O9H)Al5 sites, their ΔE_i were approximately −37 kJ/mol. The other species with ΔE_i less than −25 kJ/mol are sorted to the third group. In Table 1 listed the calculated energies based on 5T cluster models related to the different TOT sites. The orientation of the bridged O–H bonds and their location environment inside the zeolite pores were also marked. Those bridged hydroxyl species, which locate in supercages, 10-MR sinusoidal channels and connecting channels with O–H bond pointing to the channels or pores, are easily accessible by reactant molecules, and therefore are attributed to the preferable B-acid sites. For Si4(O6H)Al5 and Si2(O9H)Al5, although they have lower substitution energies, their O–H bond orientations do not direct to the channels, so they are less realistic B-acid sites. In practice, the commonly synthesized MCM-22 zeolites have Si/Al ratio of 15–30, corresponding to 4–2 framework Al atoms per unit cell, one can expect a localization selectivity for Al substitutions, because we believe the framework aluminum are not randomly distributed the lattice. In terms of above considerations, we propose Al1(O3H)Si4, Si1(O3H)Al4, and Si2(O11H)Al3 for the preferable B-acid sites, in which the first two sites locate at the intersection between the supercages and the 10-MR connecting channels or the external surface of MCM-22, and Si2(O11H)Al3 site exists at the intersection of the sinusoidal channels.

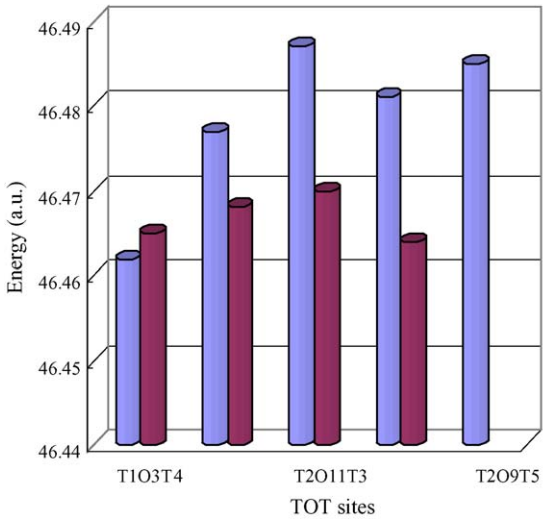

Fig. 2. The calculated (Al,H)/Si substitution energies (a.u.) for different TOT centers based on 8T cluster model in MCM-22 zeolites.

In order to obtain more accurate results and to explore the lattice configuration factors influencing the B-acidity, we have done further calculations with 8T cluster model centered with TOT bridged group related to T1, T2, T3, T4, T5, and T8 sites. All selected models are sorted to five groups. Each one contains the same framework structure, but Al atom replaced the left or the right T site of the TOT bridge, producing the substituted forms of Al(OH)Si or Si(OH)Al. The calculated substitution energies for some of TOT sites are shown in Fig. 2. The left and the right columns of each pair represent respectively the substituted form of Al(OH)Si and Si(OH)Al. From Fig. 2 one can see that Al1(O3H)Si4 and Si1(O3H)Al4 sites show lower substitution energies, while the sites related to Al2 give higher substitution energies. T3 located on the hexagonal prism between two supercages delivers two kind of bridged hydroxyl groups, Si2(O11H)Al3 and Al3(O12H)Si3. Our calculated results indicated that O–H group on Al3(O12H)Si3 bridge was pointing to the cavity of supercages, while O–H group on Si2(O11H)Al3 bridge was pointing to the sinusoidal channels. The substitution energy of Si2(O11H)Al3 was 44 kJ/mol lower than that of Si3(O12H)Al3, implying that the former is the preferred site for acidic proton. The case related to Al5 was excluded due to our previous argument. For Al substitution at T8, the calculated substitution energy showed a good stability, but Al8–O5–Si7 bond angle changed from 180° to 173.0° with fixed O5 atom and to 163.5° with relaxed O5 atom, respectively. That implies that the replacement of Si by Al at T8 may induce the distortion of the lattice framework. On this view, T8 site is unfavorable for Al location. According to above results, three protonic acid sites are confirmed for the preferable B-acid sites: Al1(O3H)Si4, Si1(O3H)Al4, and Si2(O11H)Al3.

Table 1
The calculated (Al,H)/Si substitution energies based on 5T cluster models and the localizations of B-acid sites in MCM-22 zeolite

T(OH)T center	E_{tot} (a.u.)	E(Al,H)/Si (a.u.)	ΔE_{rel} (kJ/mol)	Location of TOT center[a]	Direction of O–H bond[a]
Al1–O2H–Si6	−1709.43287	46.48180	−37.0	¦	⊥
Al1–O3H–Si4	−1709.44415	46.47052	−66.6	☼	⊥
Al1–O4H–Si7	–	–	–	▲	▲
Al2–O9H–Si5	−1709.40502	46.48933	−19.2	☼	‖
Al2–O10H–Si8	−1709.40676	46.48759	−21.8	◊	⊥
Al2–O11H–Si3	−1709.40700	46.48735	−22.4	◊	⊥
Al3–O11H–Si2	−1709.42907	46.47766	−47.8	◊	⊥
Al3–O12H–Si3	−1709.41506	46.49059	−13.9	☼	‖
Al3–O13H–Si3	−1709.41361	46.49204	−10.1	◊	⊥
Al4–O3H–Si1	−1709.44078	46.47375	−58.1	☼	⊥
Al4–O6H–Si5	–	–	–	☼	‖
Al4–O7H–Si4	−1709.42811	46.48647	−24.7	¦	⊥
Al5–O6H–Si4	−1709.42529	46.48157	−37.6	☼	‖
Al5–O8H–Si5	−1709.41098	46.49588	0	◊	⊥
Al5–O9H–Si2	−1709.42518	46.48168	−37.3	☼	‖

[a] (¦) 10-MR connecting channel, (☼) supercage, (▲) framework, (◊) sinusoidal channel, (⊥) pointing to the channel or the pore, and (‖) lie on the framework wall.

3.2. Proton affinity and atomic charge on proton

The acidity of B-acid can be predicted from the calculated proton affinity (PA) of zeolite models. Models that exhibit a high PA are poor proton donors and, therefore, have low Brönsted acidity. The PA of protonic acid in zeolite can be reasonably approximated by the deprotonation energy (ΔE_{dp}) corresponding to the reaction:

$$\text{Zeo–OH} \rightarrow \text{Zeo–O}^- + \text{H}^+$$

$$\Delta E_{dp} = E(\text{Zeo–O}^-) - E(\text{Zeo–OH})$$

The calculated ΔE_{dp} for models denoting different T sites are shown in Fig. 3. In this section we just focused on the B-acid sites with better stability. It can be seen that Al1(O3H)Si4 and Si1(O3H)Al4 sites have equivalent PA values, whereas Si2(O11H)Al3 is 10 kJ/mol higher. Our results reveal that the acidity at Si2(O11H)Al3 site is slightly weaker than Al1(O3H)Si4 and Si1(O3H)Al4 sites. As one would expect from simple chemical arguments, the sites with the lowest (Al,H)/Si substitution energy associate closely with the sites of highest PA. However, our calculation results did not follow this rule very well. A reversed case was found for Si2(O11H)Al3 site. This fact may be explained by the influence of the various lattice configurations around TOT center, which affect SiOAl anion and neutral SiOSi center through short- or long-range factors, varying from site to site.

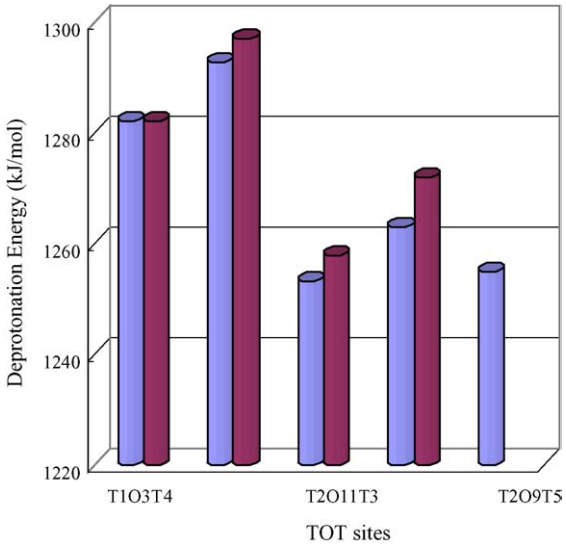

Fig. 3. The calculated deprotonation energies (kJ/mol) for different TOT centers based on 8T cluster model in MCM-22 zeolites.

Another measure for B-acidity is the atomic charge on proton, which represents the ease that an O–H bond dissociates heterolytically. The larger the q_H and the O–H distance, the stronger the B-acidity. In Table 2 listed the calculated proton charges and O–H bond distances for different optimized models. Both of Mulliken and NBO charges were obtained for comparison. It is commonly accepted that NBO charge is more reliable than Mulliken charge. This has been confirmed in our calculations in which the longer O–H bond distance is correlated to the larger NBO charge on proton. From the data in Table 2 we can see that for Al1(O3H)Si4 and Si1(O3H)Al4, their q_H and O–H bond distance are approximately same, indicating a similar acid strength. In the case of Si2(O11H)Al3, both O–H bond distance and NBO charge q_H are slightly larger than other O–H groups, implying a stronger acidity at this site. This is contrary to the conclusion from PA calculations. We will discuss it in following sections.

3.3. Calculated O–H stretching frequencies

A lower O–H stretching frequency implies a weaker O–H bond strength and the O–H group behaves as a stronger acid. In this work, frequency calculations were based on the constrained cluster model. The calculated OH stretching frequencies ν(OH) from part of bridged hydroxyls involving different surrounding configurations are listed in Table 3. The scaling factor in our present work was taken as 0.948 [29]. The corrected frequencies for Al1(O3H)Si4 and Si1(O3H)Al4 were 3628 cm^{-1} and 3617 cm^{-1}, respectively, excellently consistent with the experimental values [25]. The corrected ν(OH) for Si2(O11H)Al3

Table 2
The calculated proton charges and the O─H bond distance (8T models)

Models	NBO charge			Mulliken charge			O─H distance (Å)
	q_H	q_O	$\lvert q_H q_O \rvert$	q_H	q_O	$\lvert q_H q_O \rvert$	
Al1–O3H–Si4	0.571	−1.147	0.655	0.392	−0.611	0.240	0.9687
Si1–O3H–Al4	0.577	−1.149	0.663	0.394	−0.612	0.241	0.9695
Si2–O11H–Al3	0.583	−1.155	0.673	0.383	−0.583	0.223	0.9708

was 3592 cm^{-1}, about 7 cm^{-1} larger than the experimental data (3585 cm^{-1}), and the mean error is less than 0.1%. Our results are in good agreement with the experimental data [16,20,25]. Onida et al. [25], using IR spectroscopy technology by N_2 and CO adsorption, have characterized three kinds of B-acid sites in supercages (3628 cm^{-1}), in sinusoidal system (3618 cm^{-1}), and on the hexagonal prisms between two supercages (3585 cm^{-1}). More experiments have also found the acidic Si(OH)Al at 3620 cm^{-1} and 3585 cm^{-1} [16,20]. Comparing with our calculated O–H stretching frequencies, we can propose that both Al1(O3H)Si4 and Si1(O3H)Al4 sites located on 12-MR would be responsible for the stronger peak at 3620 cm^{-1} in IR spectrum, and the B-acid site in sinusoidal system is assigned to Si2(O11H)Al3, which locates at the intersection of sinusoidal channels and is responsible for the weak band at 3575 cm^{-1} in IR spectrum. Fig. 4 shows the proposed locations of the preferable B-acid sites in MCM-22 zeolite. Here we have to notice that Si2(O11H)Al3 bridged group is linked to the hexagonal prism, other than locates on it with O–H bond pointing to the supercages, as proposed by other researchers [20,25]. In addition, we must take caution in assigning Si2(O11H)Al3 site as a stronger acid site merely based on its comparatively smaller ν(OH) value. The larger Si2–O11–Al3 bond angle and the structural tension in surrounding lattice may account for the smaller ν(OH)value. In spite of the conflict between ν(OH) and acidity, a good correlation between Si(OH)Al bond angles and ν(OH) were found for all models in our calculations. The larger the Si(OH)Al bond angle, the lower the calculated ν(OH)s. In Table 3 one can see that for T1(O3H)T4, T2(O11H)T3, and T2(O9H)T5, no matter which T site is replaced by Al, the ν(OH) values decrease with increased T–O–T angles, depending neither on the local chemical structures, i.e. Si(OH)Al or Al(OH)Si form, nor on the surrounding configurations around TOT center. It further reveals the short-range factors playing a crucial role on the O–H stretching vibrational frequency of B-acid.

Table 3
The calculated O─H bond stretching frequencies (cm^{-1}) and Al–O–Si bond angle (°) based on 8T cluster models in MCM-22

TOT center	6-31G**/ (×0.948)	Al–O–Si angle (°)	Experimental values (Ref. [25])
Al1–O3H–Si4	3827/(3628)	131.7	
Si1–O3H–Al4	3816/(3618)	134.6	3628 for supercage
Si2–O11H–Al3	3789/(3592)	138.7	3610 for sinusoidal channel
Al2–O11H–Si3	3785/(3588)	139.0	
Al2–O9H–Si5	3714/(3521)	143.9	3585 for hexagonal prism
Si2–O9H–Al5	3648/(3458)	145.8	

The results from our calculations showed a poor correlation between proton affinities, atomic charges on proton and O–H stretching frequencies to account for B-acidity, especially for the bridging hydroxyl groups with different lattice environments. Perhaps some of the differences can be attributed to the finite cluster models, or not fully optimizing the zeolite framework structures. However, there is a better correlation for each couple of TOT sites with the same surrounding configuration. This reveals that zeolite framework structure plays an important role in the properties of proton affinity and O–H stretching frequency. Numbers of pervious works have been done for investigating the dependency of intrinsic acidity of zeolites on the short- and the long-range factors, and found that the calculated values depend on the model size in model cluster methods. Now it has been noticed by many researchers that the cluster model method cannot include the zeolite geometric features and the long-range factor of the framework (electrostatic effects), also the clusters were treated as isolated molecules with terminating hydrogen and restricted external shell frameworks. Some of possible approaches are use of hydrid methods such as embedded cluster [46–48] or QM/MM methods [49–51]. Recently, Lo and Trout [52] used periodic models of chabazite to investigate the acid strength and its relationship with the zeolite geometric properties. They found that the calculated deprotonation energy is not correlated to the O–H bond length or vibrational stretching frequency. Sillar and Burk [53] used ONIOM method including

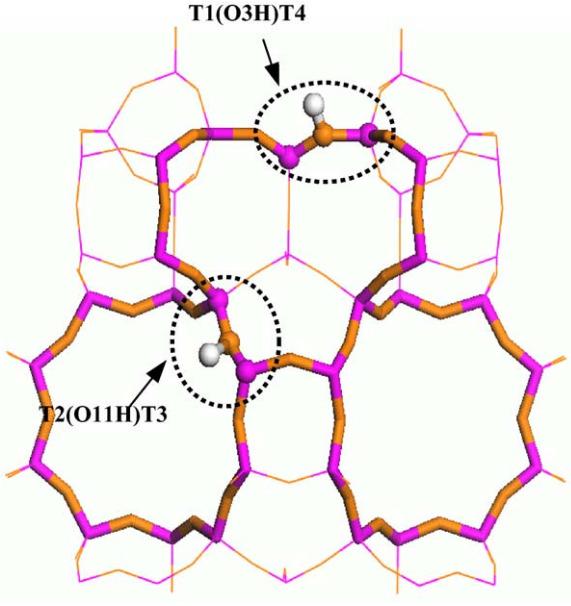

Fig. 4. Scheme for the location of B-acid sites in MCM-22 zeolite.

Table 4
The calculated interaction energies between the adsorbing bases and the acidic center based on 8T cluster models (kJ/mol)

	NH_3	C_5H_5N	C_2H_4	N_2
Al1–O3H–Si4	122.82	111.77	102.66	15.52
Si1–O3H–Al4	126.23	110.69	101.80	15.18
Si2–O11H–Al3	104.60	79.26	87.98	10.50
Al2–O11H–Si3	111.56	81.52	89.79	11.20

159–176 atoms to study the properties of the acid sites in different crystallographic positions of zeolite ZSM-5. Their results showed poor correlation between the deprotonation energy and O–H stretching vibrational frequency. However, the differences in properties of the acid sites in different crystallographic positions are better resolved in interaction with carbon monoxide permitting better comparison between the computational and experimental results. So, it is necessary to measure the B-acid strength using the adsorption energy of basic probe molecule.

3.4. Interaction with different adsorbing probe molecules

In this work, ammonia, pyridine, nitrogen, and ethene molecules are selected as probes to measure the acid strength of different protonic acid centers by calculating their interaction energies and the perturbation on the O–H bond. The interaction energy is defined as the energy difference before and after absorption of the probe molecule (B): $E_{int} = E(Z–OH) + E(B) - E(Z–OH\cdots B)$. All calculated results are listed in Table 4. No zero-point energy corrections and basis set superposition errors (BSSE) were considered. It can be seen that for all types of adsorbents, the interaction energies on Al1(O3H)Si4 and Si1(O3H)Al4 are equivalent, whereas on Si2(O11H)Al3 is slightly lower than others. These results reveal that the strength of protonic acid in supercages is relatively stronger than in 10-MR sinusoidal systems, which is in good agreement with the experiments. The interaction energies of basic probes at Si2(O11H)Al3 and Al2(O11H)Si3 are similar, revealing that the adsorption is more affected by zeolite structure than by chemical constitution. The calculations of interaction energy for four different types of probe molecules lead to accordant conclusions. The perturbation of the weak base (nitrogen and ethane) adsorption on the O–H bond length and O–H stretching vibrational frequencies were shown in Table 5.

3.4.1. Interaction with ammonia and pyridine

Ammonia and pyridine are both basic molecules, but exhibit obviously different spatial features. It can be indicated by the equilibrium geometry of ZOH—NH_3 that NH_3 become protonated in contact with zeolite cluster models, with two hydrogen atoms pointing to two lattice oxygen atoms adjacent to Al atom. The distances between the hydrogens and the lattice oxygens are equivalent. A similar configuration has been obtained by Yuan et al. [34] in their calculations on ammonia adsorption on the acid site of ZSM-5. Using microcalorimetry Dragoi et al. [54] have determined the differential heat of ammonia adsorption on H-MCM-22 and H-ZSM-5. They found the average adsorption heats of 115 kJ/mol for H-MCM-22 and 118 kJ/mol for H-ZSM-5. Our calculations have gotten the interaction energies of 122 kJ/mol on both T1 and T4 sites and 104 kJ/mol on T3 site for MCM-22, showing good agreement with the experimental data.

Pyridine adsorption formed $PyH^+–Z^-$ complex (see Fig. 5). During the course of the optimization, the proton on zeolite was transferred to pyridine, resulting in a zwitterionic complex between protonated pyridine and the zeolite anion. The hydrogen on the carbon neighbored to nitrogen in pyridine was close to the bridged oxygen adjacent to the B-acid center. Meloni et al. [20] have predicted this configuration in their experiment, and have determined the differential heats of 140–150 kJ/mol by microcalorimetry. Our calculations obtained the interaction energies of 111 kJ/mol on T1 and T4, and 79 kJ/mol on T3. Due to the larger volume of pyridine molecule and its adsorbing configuration, the spatial resistance limited its interaction on the structural restricted Si2(O11H)Al3 site(Fig. 5d). This result explains the experimental find [20] that the band at 3575 cm^{-1} reduced only slightly after adsorbing pyridine, suggesting the related protonic acid site interacted weakly with pyridine.

3.4.2. Interaction with nitrogen

Nitrogen adsorption was studied because of its weak base nature and small size. The obtained stable adsorption complexes are the H-bonded species with slightly elongated O–H bond length. The lower adsorption energies at T1, T4, and T3 of 10–15 kJ/mol indicate the weak interaction. The calculated shift in O–H bond stretching vibrational frequency, after interaction of the probe molecule with the bridged hydroxyl group, can be reliably used as a measure of the strength of hydroxyl bond, which in turn is correlated with the acidity of the acid sites [40,55]. The obtained $\Delta\nu_{OH}$ value at T1 and T4 are $-126\,cm^{-1}$ and $-139\,cm^{-1}$, respectively, in good agreement to the experiment by Onida et al. [25]. They found that the adsorption of nitrogen at 77 K resulted in the red shift of 3626 cm^{-1} ($\Delta\nu_{OH} \sim -120$ cm^{-1}, width 70 cm^{-1}). The $\Delta\nu_{OH}$ value at T3 site from our calculation is -97 cm^{-1}, however, no obvious shift was found in the experiment [25].

3.4.3. Interaction with ethene

During methane dehydro-aromatization on Mo/H-MCM-22 catalyst, ethene molecules may as intermediates go through oligomerization reaction to produce benzene [6]. The catalytic performance depends on the acid strength of protonic acid sites. In this work, we have calculated the interaction energies of ethene on different B-acid sites and listed in Table 4. For all acid sites, the stable adsorbed configurations were the H-bonded complexes, in which the symmetry plane of the π orbital of ethene molecule was quasi-perpendicular to the axis of bridged hydroxyl. Our obtained geometry is similar to the form from the experimental [56,57] and calculated results [40] for ZSM-5 zeolite. In Table 4 it can be seen that the interaction energies of C_2H_4 molecules at T1 and T4 sites are equivalently 102 kJ/mol, while at T3 site is 88 kJ/mol. Furthermore, the O–H bond at T1 and T4 sites elongated 0.02 Å, and the value of $\Delta\nu_{OH}$ was found as $-428\,cm^{-1}$ and $-433\,cm^{-1}$, similar to

Table 5
The values of the distances and stretching frequencies of O—H bond before and after adsorbed with N_2 and C_2H_4 probe

	d(O—H) (Å)	d'(O—H) (Å)	Δd(O—H) (Å)	ν(O—H) (cm^{-1})	ν'(O—H) (cm^{-1})	$\Delta\nu$(O—H) (cm^{-1})
Al1–O3H–Si4 + N_2	0.969	0.975	0.006	3827	3701	−126
Si1–O3H–Al4 + N_2	0.969	0.976	0.007	3816	3677	−139
Si2–O11H–Al3 + N_2	0.971	0.976	0.005	3789	3692	−97
Al1–O3H–Si4 + C_2H_4	0.969	0.989	0.020	3827	3401	−428
Si1–O3H–Al4 + C_2H_4	0.969	0.990	0.021	3816	3383	−433
Si2–O11H–Al3 + C_2H_4	0.971	0.983	0.012	3789	3542	−247

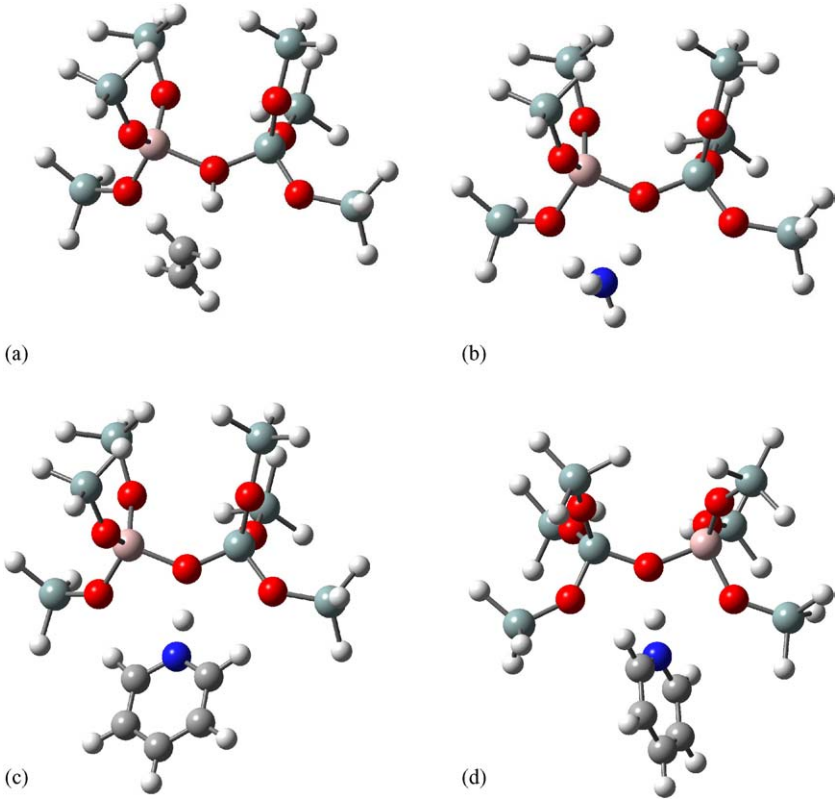

Fig. 5. Calculated structures of adsorbing complexes of the basic probes on the B-acid sites of MCM-22 Zeolite. (a) Ethene on Al1(O3H)Si4, (b) ammonia on Si2(O11H)Al3, (c) pyridine on Al1(O3H)Si4, and (d) pyridine on Si2(O11H)Al3.

the value observed experimentally by Onida et al. ($-390\,cm^{-1}$) [25]. O'Malley and Franworth have reported the calculated harmonic vibrational shift for the O–H bond of $-307\,cm^{-1}$ for ZSM-5 [58], the result compared with the experimental value of $-389\,cm^{-1}$[56]. In the case of T3 site, a remarkably low $\Delta\nu_{OH}$ value ($-247\,cm^{-1}$) was obtained, indicating a weaker interaction with ethene. These results indicate that the B-acid centers in the supercages of MCM-22 are more favorable for the catalytically oligomerization of ethene. Based on our results it is concluded that the stronger Brönsted acid site correlate to both Al1(O3H)Si4 and Al4(O3H)Si1, while relative weaker site locate at Al3(O11H)Si2.

4. Conclusions

DFT method was used to study the location of framework aluminum atom in MCM-22 zeolite, and the preferable Brönsted acid sites as well as the acidity were predicted. The substitution energies of Al at eight inequivalent T sites were calculated using the cluster models in form $T(OSiH_3)_4$ and $(H_3SiO)_3TOT(OSiH_3)_3$, defined as 5T and 8T models, respectively. B3LYP hydride functional and 6-31G** basis set were used.

8T model is confirmed to be adequate for evaluation of protonic acidity of zeolites, which can reflect the medium- and short-range effectors of the lattice on the intrinsic acidity of B-acid. The calculations reveal that protonic acidity depends extremely on the configuration of lattice environment around the TOT group. Better correlations are found for each couple of TOT sites with the same kind of environment. In this case, the substitution of different T sites to Al atom leads to different stability and acidity. The difference in (Al,H)/Si substitution energies is larger than that of proton affinities. The measurements from PA, ν(OH), q_{H^+}, E_{int} are in good consistent with each other for

evaluation of the intrinsic acidity. Whereas, for the TOT group with different lattice environments, no linear relationships have been found for PA and ν(OH). Nevertheless, PA's are well consistent with the interaction energies of B-acid sites and adsorbed basic molecules. The interaction energy depends not only on the acid–base action, but also on the multiple interactions between zeolite frameworks and basic molecule. The latter involve spatial effect, i.e. the steric hindrance at the acidic centers. Therefore, the calculated interaction energies with appropriate models can reflect the short- and medium-range factors, are more reasonable for measuring the acidity of B-acid with different kind of environments and in different zeolites.

From calculated (Al,H)/Si substitution energies it was predicted that the most favorable sites for Al substitution in MCM-22 are T1, T3, and T4 sites, whereas the least favorable site is T2. It further reveals that the most preferable Brönsted acid sites locate on Al1(O3H)Si4, Al4(O3H)Si1, and Al3(O11H)Si2. The first two situate on the pocket edge of 12-MR supercages with bridged O–H group pointing to 10-MR connecting channel, which also attributed to the external surface acid sites. The third one exists at the intersection of sinusoidal channels with bridged O–H group pointing to the pores. Based on the interaction energies with different basic probe molecules, we can confirm that the acidities of Al1(O3H)Si4 and Al4(O3H)Si1 sites are equivalent and stronger than that of Al3(O11H)Si2 site. Through our calculations, no stable bridge hydroxyl groups were found inside supercage pockets.

Acknowledgments

The authors are grateful to the National Nature Science Foundation of China (No.90206036) and the Education Ministry of Liaoning (No. 202122025) for the financial support.

References

[1] M.E. Leonowicz, J.A. Lawton, S.L. Lawton, M.K. Rubin, Science 264 (1994) 1910.
[2] S.L. Lawton, M.E. Leonowicz, R.D. Partridge, P. Chu, M.K. Rubin, Microporous Mesoporous Mater. 23 (1998) 109.
[3] M. Cheng, D. Tan, X. Liu, X. Han, X. Bao, L. Lin, Microporous Mesoporous Mater. 31 (1999) 241.
[4] M.J. Verhoef, E.J. Creyghton, J.A. Peters, H. Van Bekkum, Chem. Commun. (1997) 1989.
[5] P. Wu, T. Komatsu, T. Yashima, Microporous Mesoporous Mater. 22 (1998) 343.
[6] A. Corma, J. Martínez-Triguero, J. Catal. 165 (1997) 102.
[7] A. Huss Jr., G.W. Kirker, K.M. Keville, R.T. Thomson, U.S. Patent 4,992,615 (1991).
[8] A. Corma, C. Corell, F. Llopis, A. Martinéz, J. Pèrez-Pariente, Appl. Catal. A 115 (1994) 121.
[9] Y. Shu, D. Ma, L. Xu, Y. Xu, X. Bao, Stud. Surf. Sci. Catal. 137 (2001) 27.
[10] A. Corma, M. Davis, V. Fornés, V. Gonzàles-Alfaro, R. Lobo, A.V. Orchillès, J. Catal. 167 (1997) 438.
[11] N. Kumar, L.-E. Lindsfors, Appl. Catal. A 147 (1994) 175.
[12] P. Mériaudeau, V.A. Tuan, V.T. Nghiem, F. Lefevbre, V.T. Ha, J. Catal. 185 (1999) 378.
[13] G.J. Kennedy, S.L. Lawton, M.K. Rubin, J. Am. Chem. Soc. 116 (1994) 11000.
[14] A. Corma, C. Corell, V. Fornés, W. Kolodziejski, J. Pérez-Pariente, Zeolites 15 (1995) 576.
[15] S. Unverricht, M. Hunger, S. Ernst, H.G. Karge, J. Weitkamp, in: J. Weitkamp, et al. (Eds.), Zeolite and Related Microporous Materials: State of the Art 1994, Studies in Surface Sciences and Catalysis, vol. 84, Part A, Elsevier, Amsterdam, 1994, p. 37.
[16] R. Ravishankar, T. Sen, S. Sivasanker, S. Ganapathy, J. Chem. Soc. Faraday Trans. 91 (1995) 3549.
[17] M. Hunger, S. Ernst, J. Weitkamp, Zeolites 15 (1995) 188.
[18] W. Kolodziejski, C. Zicovich-Wilson, C. Corell, J. Pérez-Pariente, A. Corma, J. Phys. Chem. 99 (1995) 7002.
[19] S.L. Lawton, A.S. Fung, G.J. Kennedy, L.B. Alemany, C.D. Chang, G.H. Hatzikos, D.N. Lissy, M.K. Rubin, H.C. Timken, S. Steuernagel, D.E. Woessner, J. Phys. Chem. 100 (1996) 3788.
[20] D. Meloni, S. Laforge, D. Martin, M. Guisnet, E. Rombi, V. Dolonas, Appl. Catal. A: Gen. 215 (2001) 55.
[21] P. Mériaudeau, A. Tuel, V.T. Ha, Catal. Lett. 61 (1999) 89.
[22] G.L. Kennedy, S.L. Lawton, A.S. Funy, M.K. Rubin, S. Steuernagel, Catal. Today 49 (1999) 385.
[23] D. Ma, F. Deng, R. Fu, X. Han, X. Bao, J. Phys. Chem. B 105 (2001) 1770.
[24] B. Onida, F. Geobaldo, F. Testa, R. Aiello, E. Garrone, J. Phys. Chem. B 106 (2002) 1684.
[25] B. Onida, F. Geobaldo, F. Testa, F. Crea, E. Garrone, Microporous Mesoporous Mater. 30 (1999) 119.
[26] J. Sauer, J. Chem. Rev. 89 (1989) 199, and references therein.
[27] J.G. Fripiat, F. Berger-andre, J.M. Andre, E.G. Derouane, Zeolites 3 (1983) 306.
[28] E.G. Derouane, J.G. Fripiat, Zeolites 5 (1985) 165.
[29] H.V. Brand, L.A. Curtiss, L.E. Iton, J. Phys. Chem. 96 (1992) 7725.
[30] J.B. Nicholas, R.E. Winans, R.J. Harrison, L.E. Iton, L.A. Curtiss, A.J. Hopfinger, J. Phys. Chem. 96 (1992) 10247.
[31] A.E. Alvarado-Swaisgood, M.K. Barr, P.J. Hay, A. Redondo, J. Phys. Chem. 95 (1991) 10031.
[32] A. Chatterjee, A.K. Chandra, J. Mol. Catal. 119 (1997) 51.
[33] A. Chatterjee, T. Iwasaki, T. Ebina, A. Miyamoto, Microporous Mesoporous Mater. 21 (1998) 421.
[34] S. Yuan, J. Wang, Y. Li, S. Peng, J. Mol. Catal. 175 (2001) 131.
[35] G. Sastre, V. Fornes, A. Corma, J. Phys. Chem. B 104 (2000) 4349.
[36] Y. Wang, J.Q. Zhuang, D.H. Zhou, D. Ma, X.W. Han, X.H. Bao, J. Phys. Chem. B 108 (2004) 1386.
[37] Y. Wang, D.H. Zhou, G. Yang, X.C. Liu, D. Ma, D.B. Liang, X.H. Bao, Chem. Phys. Lett. 388 (2004) 363.
[38] Ch. Baerlocher, W.M. Meier, D.H. Olson, Atlas of Zeolite Framework Types, fifth ed., Elsevier, Amsterdam, 2001.
[39] Cerius 2, Version 4.2, Dmol 3, Molecular Simulations Inc., 2000.
[40] P.J. O'Malley, K.J. Farnworth, J. Phys. Chem. B 102 (1998) 4507.
[41] M.J. Rice, A.K. Chakraborty, A.T. Bell, J. Phys. Chem. A 102 (1998) 7498.
[42] B.G. Johnson, P.M.W. Gill, J.A. Pople, J. Chem. Phys. 98 (1993) 5612.
[43] C. Sosa, J. Andzelm, B.C. Elkin, E. Winner, K.D. Dobbs, D.A. Dixon, J. Phys. Chem. 96 (1992) 6630.
[44] C.W. Murray, G.J. Laming, N.C. Handy, R.D. Amos, J. Phys. Chem. 97 (1993) 1868.
[45] J. Hutter, H.P. Luthi, F. Diederich, J. Am. Chem. Soc. 116 (1994) 750.
[46] S.J. Cook, A.K. Chakraborty, A.T. Bell, D.N. Theodoru, J. Phys. Chem. 97 (1993) 6679.
[47] J.M. Vollmer, E.V. Stefanovich, T.N. Truong, J. Phys. Chem. B. 103 (1999) 9415.
[48] J. Limtrakul, P. Khongpracha, S. Junsuttiwong, T.N. Truong, J. Mol. Catal. 153 (2000) 155.
[49] M. Svensson, S. Humbel, R.D.J. Froese, T. Matsubara, S. Sieber, K. Morokuma, J. Phys. Chem. 100 (1996) 19357.
[50] S. Humbel, S. Sieber, K. Morokuma, J. Chem. Phys. 105 (1996) 1959.
[51] K. Sillar, P. Burk, Chem. Phys. Lett. 393 (2004) 285.
[52] C. Lo, B.L. Trout, J. Catal. 227 (2004) 77.

[53] K. Sillar, P. Burk, J. Mol. Struct. (Theochem.) 589–590 (2002) 281.
[54] B. Dragoi, A. Gervasini, E. Dumitriu, A. Auroux, Thermochim. Acta 420 (2004) 127.
[55] J. Datka, J. Chem. Soc. Faraday Trans. 77 (1981) 511.
[56] G. Spoto, S. Bordiga, G. Ricchiardi, D. Scarano, A. Zecchina, E. Borello, J. Chem. Soc. Faraday Trans. 90 (1994) 2827.
[57] J.L. White, L.W. Beck, J.F. Haw, J. Am. Chem. Soc. 114 (1992) 6182.
[58] P.J. O'Malley, K.J. Franworth, J. Phys. Chem. 102 (1998) 4507.